Supporting Information

Imido Ligand Significantly Enhances The Effective Energy Barrier of Dysprosium(III) Single-Molecule Magnets

Bing-Cheng Liu[‡, a], Ning Ge[‡, a], Yuan-Qi Zhai[‡, a], Tao Zhang[a] You-Song Ding[a] and Yan-Zhen Zheng[, a]*

[a] *Frontier Institute of Science and Technology (FIST), State Key Laboratory for Mechanical Behaviour of Materials, MOE Key Laboratory for Nonequilibrium Synthesis of Condensed Matter, Xi'an Key Laboratory of Sustainable Energy and Materials Chemistry and School of Science Xi'an Jiaotong University, 99 Yanxiang Road, Xi'an, Shaanxi 710054, P. R. China.*

Email: zheng.yanzhen@xjtu.edu.cn

[‡] These authors contributed equally in this work.

Experimental sections

Unless otherwise stated, all reagents were purchased from commercial suppliers and used as is. All solvents were dehydrated and deoxygenated using a solvent purification system prior to use. The synthesis of the compounds involved in the experiments was performed either via a Schlenk line or under argon in a glove box. The single crystals were encapsulated with deoxygenated crystal oil and all single crystal data were collected on a Bruker SMART APEX II CCD diffractometer using a molybdenum target (MoKα, λ = 0.71073Å). The resulting data was refined and analyzed using Olex2. X-ray powder diffraction was tested by Rigaku SmartLab. The samples were sealed in a polyethylene bag and magnetic measurements were made on a Quantum Design MPMS-XL7 SQUID with data collection from 2 to 300 K and applied DC fields of 0 to +7 T.

1. Materials

Anhydrous $DyCl_3$ salts, NaOAr* and $Im^{Dipp}NH$ were prepared according to literature procedures[1, 2, 3]. These two complexes were synthesized under a dry and oxygen-free argon atmosphere in a glovebox. THF, Toluene and hexane were dried and degassed by standard techniques.

2. Synthesis

2.1. Synthesis of 1,3-bis(2,6-diisopropylphenyl)-imidazolin-2-imine ($Im^{Dipp}NH$)

2,6-Diisopropylaniline 10ml(53mmol) and glyoxal 2.87ml(26mmol) with 100ml methyl alcohol, stir over night. After the reaction is complete, a large number of microcrystalline bright yellow solids are precipitated out, and the solid-liquid separation is completed by filtration with a sand core funnel. Get the product 8.8g, Yield:90%, ^{1}H NMR (300 MHz, $CDCl_3$): δ 8.11 (s, 2H), 7.25–7.11 (m, 6H), 2.94 (sept, 4H, *J* = 6.9 Hz) and 1.21 (d, 24H, *J* = 6.9 Hz).^{13}C-{^{1}H} NMR (85 MHz, $CDCl_3$): δ 163.0, 148.0, 136.6, 125.1, 123.1, 28.1 and 22.4.

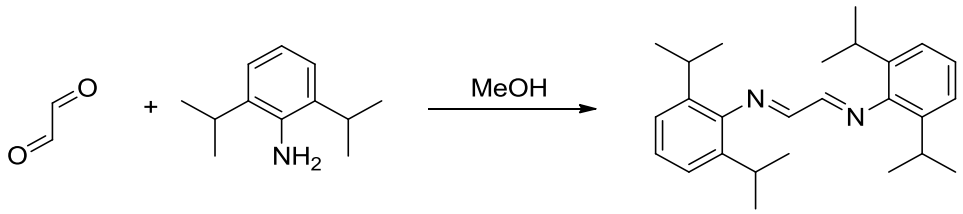

Scheme S1. Synthesis of the N,N-μ-Bis(2,6-diisopropylphenyl)ethanediimine.

In a round-bottom flask, dissolve N,Nμ-Bis(2,6-diisopropylphenyl)ethanediimine 3.76g(10mmol) in 100ml ethyl acetate. In a conical flask, weigh out 0.33g(11mmol) of paraformaldehyde and transfer 3.5 ml of HCl (4 M in dioxane). Stir the mixture until paraformaldehyde dissolves and gives a clear solution. Transfer the solution of paraformaldehyde to the round-bottom flask. After overnight reaction, the solution gradually turns dark reddish-brown and slowly becomes turbid. The collected solids were washed with a small amount of ethyl acetate (3×10ml) to obtain the grey-white solids, and dried to obtain the products 2.76g. Yield: 65%,^{1}H NMR (400 MHz, CD_2Cl_2): δ 11.25 (s, 1H), 7.76 (d, 2H, *J* = 1.5 Hz), 7.62 (t, 2H, *J* = 7.8 Hz), 7.39 (d, 4H, *J* = 7.8 Hz), 2.43 (sept, 4H, *J* = 6.8 Hz), 1.28 (d, 12H, *J* = 6.6 Hz) and 1.27 (d, 12H, *J* = 6.7 Hz).^{13}C-{^{1}H} NMR (100 MHz, CD_2Cl_2): δ 145.5, 141.2, 132.3, 130.5, 125.9, 125.0, 29.5, 24.8 and 23.7.

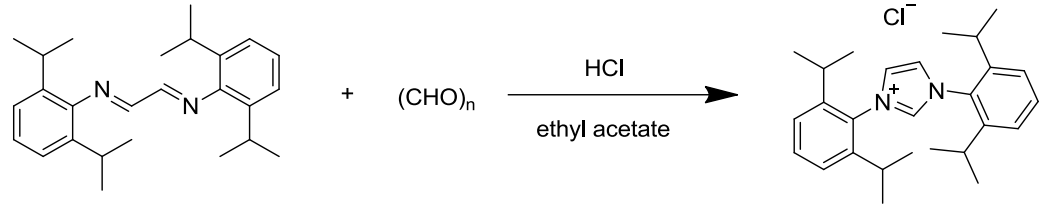

Scheme S2. Synthesis of the 1,3-Bis(2,6- diisopropylphenyl)imidazoliumchloride.

In a glovebox, 4.25g(10mmol) 1,3-Bis(2,6- diisopropylphenyl)imidazoliumchloride and 1.42g(12mmol) KO^{t}Bu are added to a round-bottom flask. Add 40ml of anhydrous THF and the solution becomes turbid. After stirring at room temperature for 4 hours, the milky white suspension gradually turned into a light green solution, and the solvent was drained under the vacuum, the off-white solid was obtained. 50ml anhydrous and anoxic toluene was added to form suspension after stirring, and slightly heated to make it uniform. Then add the anhydrous anoxic hexane, a large amount of white precipitation. The filtrate appears light yellow, and the collected filtrate is drained to obtain a microcrystalline colorless solid 3.5g, Yield: 90%,^{1}H NMR (300 MHz, C_6D_6): δ 7.29 (t, 2H, *J* = 7.5 Hz), 7.18 (d, 4H, *J* = 7.5 Hz), 6.62 (s, 2H), 2.96 (sept, 4H, *J* = 6.9 Hz), 1.28 (d, 12H, *J* = 6.9 Hz) and 1.18 (d, 12H, *J* = 6.9 Hz).^{13}C-{^{1}H} NMR (85 MHz, $CDCl_3$): δ 220.6, 146.2, 139.0, 129.0, 123.6, 121.5, 28.7, 24.8 and 23.6.

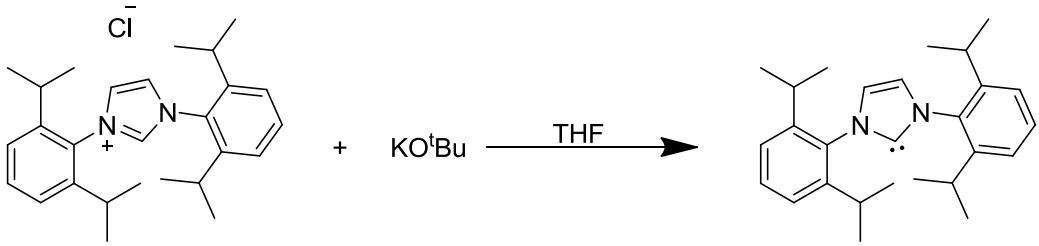

Scheme S3. Synthesis of the 1,3-Bis(2,6-diisopropylphenyl)imidazol-2-ylidene.

A solution of the respective 1,3-Bis(2,6-diisopropylphenyl) imidazol-2-ylidene 3.9g (10 mmol) in toluene (20 mL) was treated dropwise with trimethylsilyl azide 2ml (14 mmol), and the resulting reaction mixture was subsequently heated in boiling toluene for 72h. Filtration and evaporation of the solvent afforded the imines as yellowish solids 4.1g at ambient temperature. Yield:90%,^{1}H NMR (400 MHz, C_6D_6) 7.21(4H, m, m-H), 7.14 (2H, s, p-H), 5.95 (2H, s, NCH), 3.18 (4H, sept, CHMe), 1.38 (12H, d, CH_3), 1.20 (12 H, d, CH_3) and −0.16(9 H, s, $SiCH_3$). ^{13}C-{^{1}H} NMR (67.93 MHz, C_6D_6) 148.0 (o-C), 141.3 (NCN),135.2 (ipso-C), 129.4 (p-CH), 123.9 (m-CH), 113.8 (CH), 28.9(CHMe), 24.4 (CHMe), 23.5 (CHMe) and 3.5 ($SiCH_3$).

Scheme S4. Synthesis of the 1,3-Bis(2,6-diisopropylphenyl)-2-(trimethylsilylimino)imidazoline.

1,3-Bis(2,6-diisopropylphenyl)-2-(trimethylsilylimino)imidazoline 4.7g (10mmol) were

treated with an excess of CH_3OH 10ml at ambient temperature for 2h. The solvent was then removed in vacuum and the product extracted with n-hexane. Filtration and evaporation of n-hexane afforded the imines as colorless solids 3.6g. Yield: 90%, ^{1}HNMR (400 MHz, C_6D_6, 25 ◦C): d 7.22 (m, 4 H, m-H), 7.14 (s,2 H, p-H), 5.87 (s, 2 H, NCH), 4.21 (br., 1 H, NH), 3.22 (sept.,4 H, CHMe), 1.35 (d, 12 H, CH_3), 1.22 (d, 12 H, CH_3) ppm. ^{13}CNMR (100.52 MHz, C_6D_6): d 159.5 (NCN), 154.6 (ipso-C), 148.6(o-C), 129.6 (p-CH), 124.3 (m-CH), 113.6 (CH), 29.0 (CHMe),24.1 ($CHCH_3$), 24.0 ($CHCH_3$) ppm.

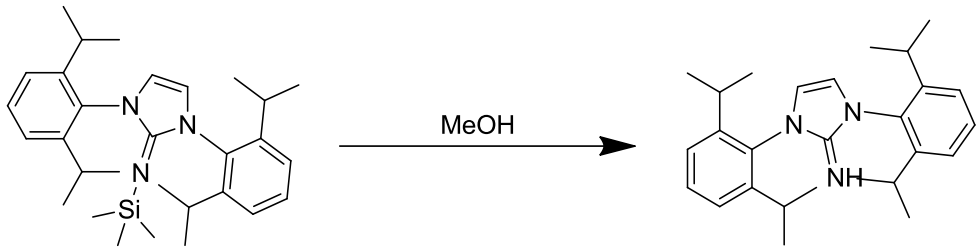

Scheme S5. Synthesis of the 1,3-Bis(2,6-diisopropylphenyl) imidazoline -2-imine.

2.2 Synthesis of the NaOAr*

In a 250 mL round-bottom flask was charged p-cresol (8 g, 74 mmol), diphenylmethanol (27g, 148 mmol), the round-bottomed flask was heated to 140ºC, and HCl/$ZnCl_2$(2.22 mL, 73.2 mmol HCl; 37mmol ZnCl2 (5.20 g)) solution was slowly added with a dropper when the reactants became molten. After stirring for half an hour, the reactant gradually thickens and begins to solidify. The reaction lasts for two hours. After the reaction is complete, cooled to room temperature. The crude product was dissolved with 50mL methylene chloride and washed once with distilled water and twice with saturated sodium chloride solution. The organic phase was collected and dried with anhydrous sodium sulfate and then the solvent was removed under the rotary evaporator. Add 50ml methanol solution, stir overnight, and filter to get white solid 27g, 61.2mmol. Yield: 84%,^{1}H NMR (270 MHz, $CDCl_3$): δ = 7.32−7.26(m, 12H, Ar-H), 7.26−7.09 (m, 8H, Ar-H), 6.50 (s, 2H, Ar-H), 5.67(s, 2H, $CH(Ph)_2$), 4.43 (s, 1H, OH), 2.07 (s, 3H, Me). 13C NMR (25ºC, 67.8 MHz, CDCl3): δ 149.05 (Ar), 142.79 (Ar), 130.77 (Ar),129.33 (Ar), 128.46 (Ar), 126.57 (Ar), 51.05 (Ph2CH), 20.97 (Me).

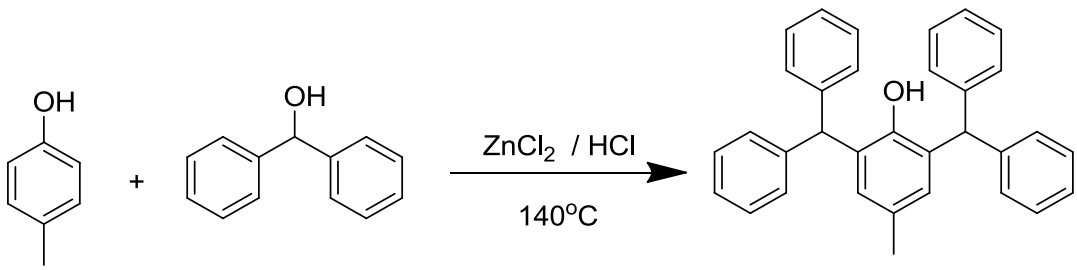

Scheme S6. Synthesis of the NaOAr*

2.3 Synthesis of complex **1**

Reaction of $DyCl_3$ (0.5 mmol, 0.268 g), $Im^{Dipp}NH$ (0.5 mmol, 0.202 g) and Me_3SiCH_2Li (0.5 mmol). The role of trimethyl silicomethyl lithium is to participate in ligand replacement. in 5 mL THF afforded the imidazolin-2-iminato complexes as colorless crystalline solids in good yield (60%) after extraction with toluene and crystallization from THF/pentane solution (1:2). Elemental analysis found (calcd.) % for $C_{44}H_{56}Cl_2DyN_3O_3$: the theoretical values are in parentheses, C, 49.73(52.12); Dy,28.48(26.46); Cl, 7.50(7.00); H,4.63(5.53); O, 5.10(4.74); N, 4.56(4.15).

2.4 Synthesis of complex **2**

Reaction of $DyCl_3$ (0.5 mmol, 0.268 g), and NaOAr* (1 mmol, 0.196 g) in 10 mL THF afforded the complex **2** as colorless crystalline solids in good yield (75%) after crystallization from THF/pentane solution (1:2). Elemental analysis found (calcd.) % for $C_{45}H_{51}Cl_2DyO_4$: the theoretical values are in parentheses, C,54.38(54.33); Dy, 25.75(26.96); Cl, 7.94(7.14); O, 6.72(6.44); H, 5.21(5.13).

3. X-ray Crystallography data

All data were recorded on a Bruker SMART CCD diffractometer with MoKα radiation (λ = 0.71073 Å). The structures were solved by direct methods and refined on F2 using SHELXTL. CCDC 1886042 (**1**) and 1886033(**2**) contains the supplementary crystallographic data for this paper. These data can be obtained free of charge via www.ccdc.cam.ac.uk/conts/retrieving.html (or from the Cambridge Crystallographic Data Centre, 12 Union Road, Cambridge CB21EZ, UK; fax: (+44)1223-336-033; or deposit@ccdc.cam.ac.uk).

Table S1: Crystallographic data for complex **1**.

Empirical formula	$C_{44}H_{56}Cl_2DyN_3O_3$
Formula weight[g mol^{-1}]	1013.1
Crystal system	monoclinic
Space group	$P2_1/n$
a [Å]	18.1751(16)
b [Å]	12.3575(11)
c [Å]	20.0341(17)
α [°]	90
β [°]	96.1852(13)
γ [°]	90
V [Å^3]	4473.4(7)
Z	4
ρ_{calc}[g cm^{-3}]	1.373
F(000)	1916
	MoKα (λ = 0.71073)
2θ range for data collection/°	3.202 to 55.326
Index ranges	$-23 \leq h \leq 23$, $-11 \leq k \leq 16$, $-26 \leq l \leq 25$
Reflections collected	41929
Independent reflections	10355 [R_{int} = 0.0411, R_{sigma} = 0.0417]
Data/restraints/parameters	10355/0/486
Goodness-of-fit on F^2	1.029
Final R indexes [I>=2σ (I)]	R_1 = 0.0310, wR_2 = 0.0638
Final R indexes [all data]	R_1 = 0.0507, wR_2 = 0.0702
Largest diff. peak/hole / e Å^{-3}	1.02/-0.38

Table S2: Selected bond lengths (Å) and angles (deg) in complex **1**.

Dy(1)-Cl(2)	2.6275(8)	Dy(1)-O(7)	2.3568(19)
Dy(1)-Cl(3)	2.6307(9)	Dy(1)-O(1)	2.3706(19)
Dy(1)-N(4)	2.121(2)	Dy(1)-O(2)	2.508(2)
N(4)-Dy(1)-O(2)	177.44(7)	O(7)-Dy(1)-Cl(2)	87.97(5)
N(4)-Dy(1)-Cl(2)	99.93(7)	O(7)-Dy(1)-Cl(3)	92.37(6)
N(4)-Dy(1)-Cl(3)	99.73(7)	O(7)-Dy(1)-O(1)	157.19(7)
N(4)-Dy(1)-O(7)	99.62(8)	O(7)-Dy(1)-O(2)	77.96(7)
N(4)-Dy(1)-O(1)	102.99(8)	O(1)-Dy(1)-Cl(2)	85.31(5)
Cl(2)-Dy(1)-Cl(3)	159.99(3)	O(1)-Dy(1)-Cl(3)	86.72(5)
O(2)-Dy(1)-Cl(2)	80.91(5)	O(1)-Dy(1)-O(2)	79.47(7)
O(2)-Dy(1)-Cl(3)	79.61(5)		

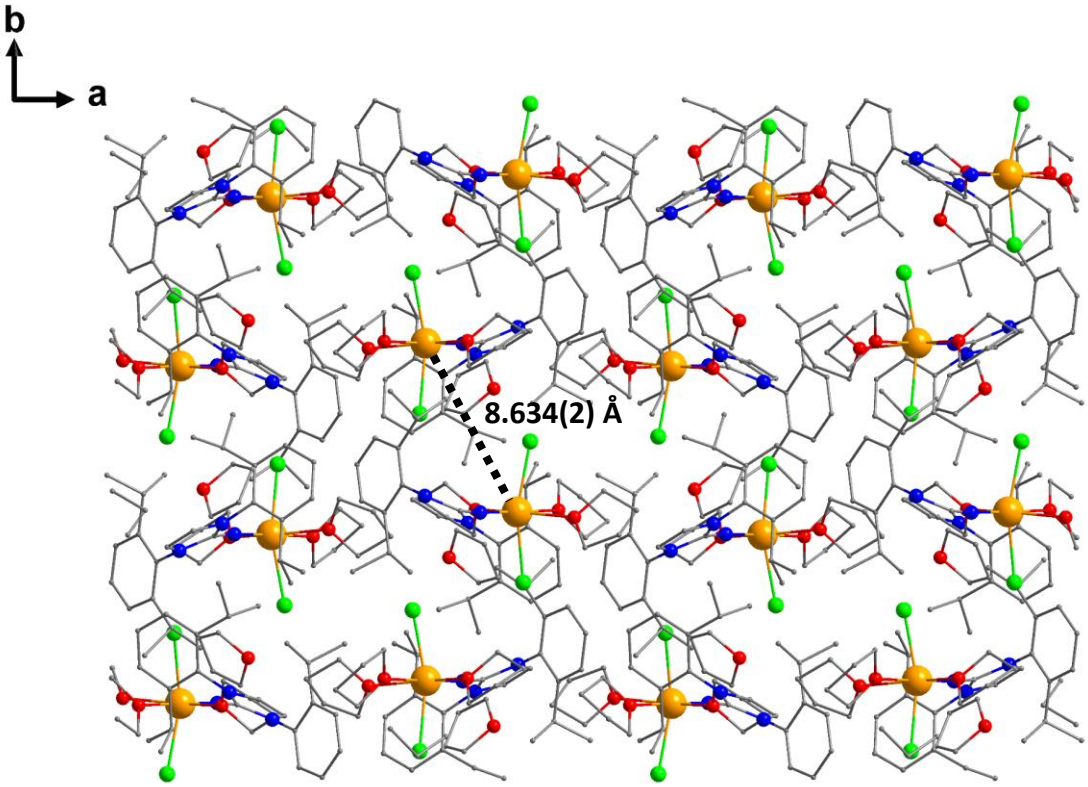

Fig. S1. The molecular packing in **1**. Color codes: Dy, gold; N, blue; O, red; C, grey; Cl, green. For clarity, hydrogen atoms in both complexes are omitted.

Table S3: Crystallographic data for complex **2**.

Empirical formula	$C_{45}H_{51}Cl_2DyO_4$
Formula weight	889.26
T[K]	150
Crystal system	monoclinic
Space group	*C*2/c
a [Å]	42.722(18)
b [Å]	8.732(4)
c [Å]	21.661(9)
α [°]	90
β [°]	94.395(9)
γ [°]	90
Volume[Å^3]	8057(6)
Z	8
ρ_{calc} [g/cm^3]	1.466
μ[mm^{-1}]	2.029
F(000)	3624.0
Radiation	MoKα (λ = 0.71073)
2ϑ range for data collection[°]	3.772 to 55.606
Index ranges	-55 ≤ h ≤ 55, -11 ≤ k ≤ 11, -28 ≤ l ≤ 28
Reflections collected	35943
Independent reflections	9308 [R_{int} = 0.0415, R_{sigma} = 0.0382]
Data/restraints/parameters	9308/60/516
Goodness-of-fit on F^2	1.091
Final R indexes [I>=2σ (I)]	R_1 = 0.0378, wR_2 = 0.0789
Final R indexes [all data]	R_1 = 0.0537, wR_2 = 0.0843
Largest diff. peak/hole [e Å^{-3}]	1.24/-1.09

Table S4: Selected bond lengths (Å) and angles (deg) in complex **2**.

Dy(01)-Cl(02)	2.6122(12)	Dy(01)-O(005)	2.374(3)
Dy(01)-Cl(03)	2.6303(12)	Dy(01)-O(006)	2.353(3)
Dy(01)-O(004)	2.088(3)	Dy(01)-O(2)	2.343(9)
Cl(02)-Dy(01)-Cl(03)	166.93(3)	O(006)-Dy(01)-Cl(02)	89.35(8)
O(004)-Dy(01)-Cl(02)	97.93(7)	O(006)-Dy(01)-Cl(03)	87.50(8)
O(004)-Dy(01)-Cl(03)	94.78(7)	O(006)-Dy(01)-O(005)	167.11(1)
O(004)-Dy(01)-O(005)	102.49(10)	O(2)-Dy(01)-O(005)	89.9(2)
O(004)-Dy(01)-O(006)	90.39(10)	O(005)-Dy(01)-Cl(03)	91.90(8)
O(2)-Dy(01)-O(006)	77.3(2)	O(2)-Dy(01)-Cl(03)	81.2(2)
O(004)-Dy(01)-O(2)	167.1(2)	O(2)-Dy(01)-Cl(02)	85.7(2)
O(005)-Dy(01)-Cl(02)	88.35(8)		

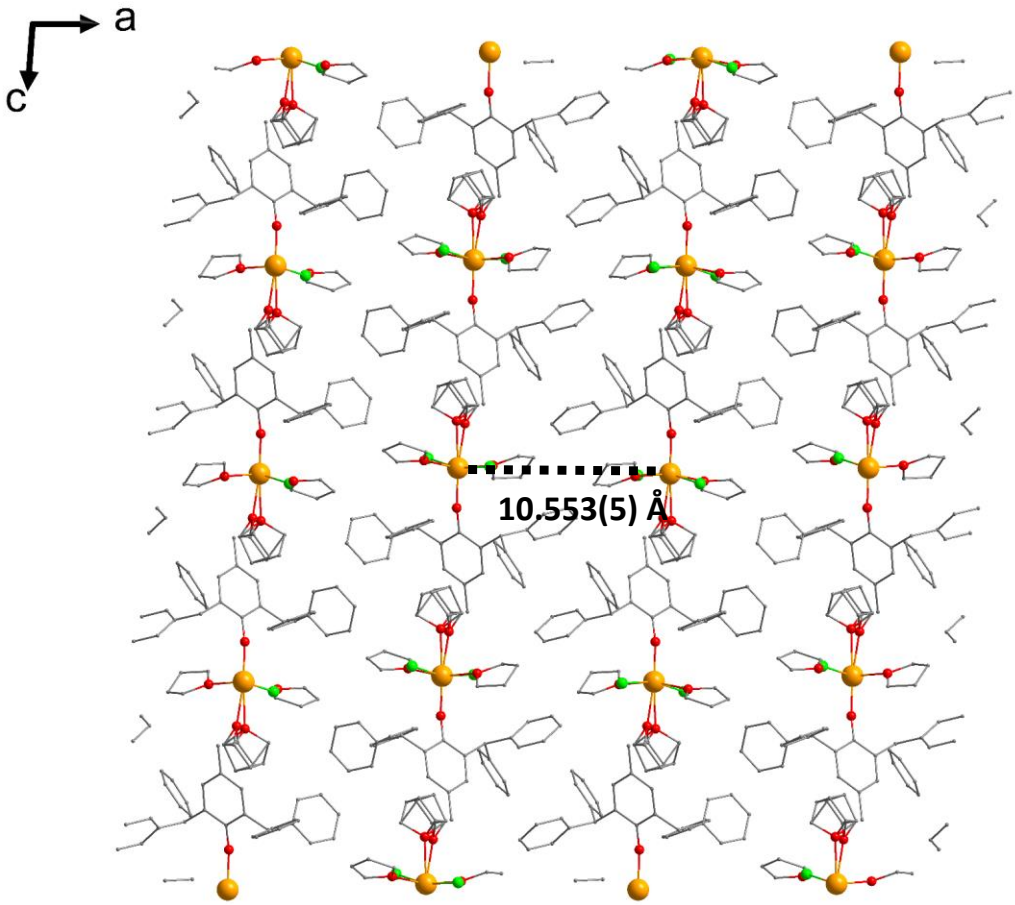

Fig. S2. The molecular packing in **2**. Color codes: Dy, gold; O, red; C, grey; Cl, green. For clarity, hydrogen atoms in both complexes are omitted.

Table S5. Continuous Shape Measures (CSM) calculation for **1** and **2**.

HP-6	1 D6h	Hexagon
PPY-6	2 C5v	Pentagonal pyramid
OC-6	3 Oh	Octahedron
TPR-6	4 D3h	Trigonal prism
JPPY-6	5 C5v	Johnson pentagonal pyramid J2

Structure [ML6]	HP-6	PPY-6	OC-6	TPR-6	JPPY-6
DyN (**1**)	33.555,	28.208,	0.960,	15.704,	31.244
DyO (**2**)	33.287,	26.844,	0.967,	15.492,	30.183

4. Magnetic Properties

Magnetic susceptibility measurements were carried out with a Quantum Design MPMS-XL7 SQUID magnetometer. Freshly prepared crystalline samples were embedded in eicosane to avoid any field induced crystal reorientation. Diamagnetic corrections have been applied for the eicosane and for the molecule, the latter being calculated from the Pascal constants.

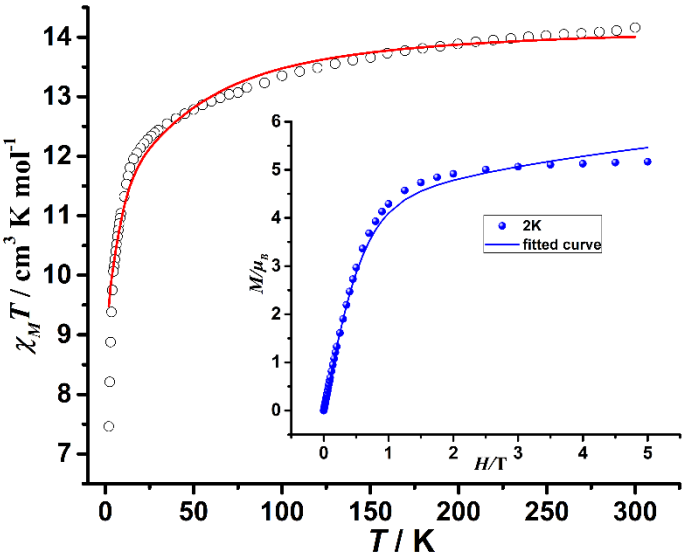

Fig. S3. Variable temperature magnetic susceptibility of complex **1**, under a field of 1000 Oe. The high temperature limit for χT is 14.16 cm^3 mol^{-1} K at 300 K. Inset: variable field magnetization of complex **1**, at temperatures of 2 K.

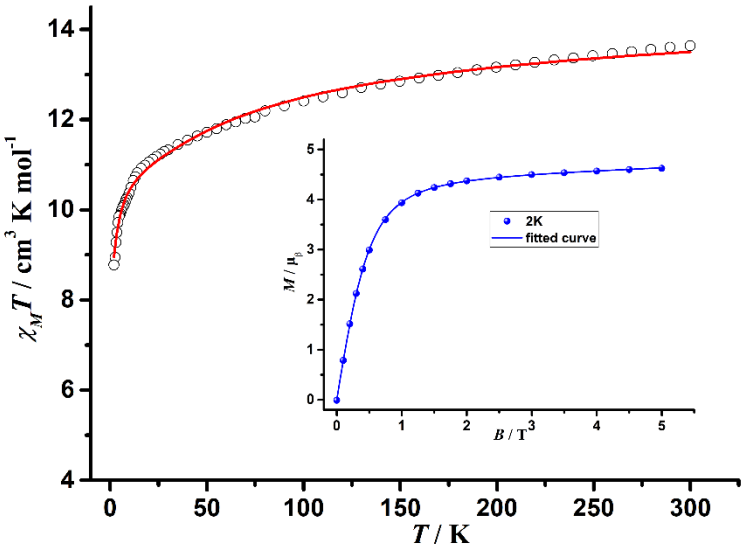

Fig. S4. Variable temperature magnetic susceptibility of complex **2**, under a field of 1000 Oe. The high temperature limit for χT is 13.64 cm^3 mol^{-1} K at 300 K. Inset: variable field magnetization of complex **2**, at temperatures of 2 K.

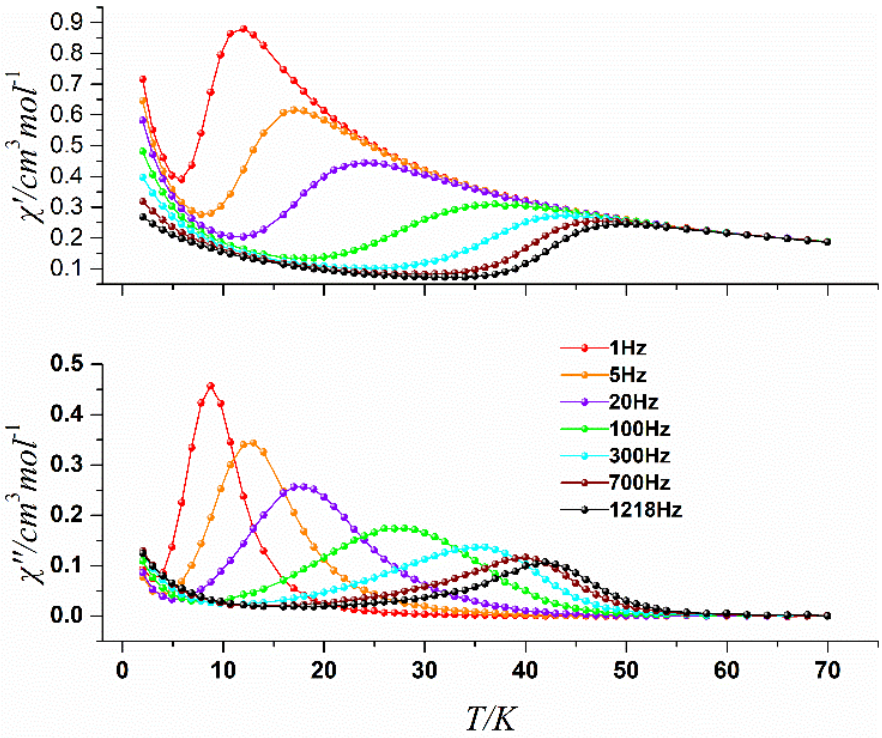

Fig. S5. Variable-temperature in-phase (top) and out-of-phase (bottom) magnetic susceptibility of **1** in zero static field and an oscillating field of 3.5 Oe.

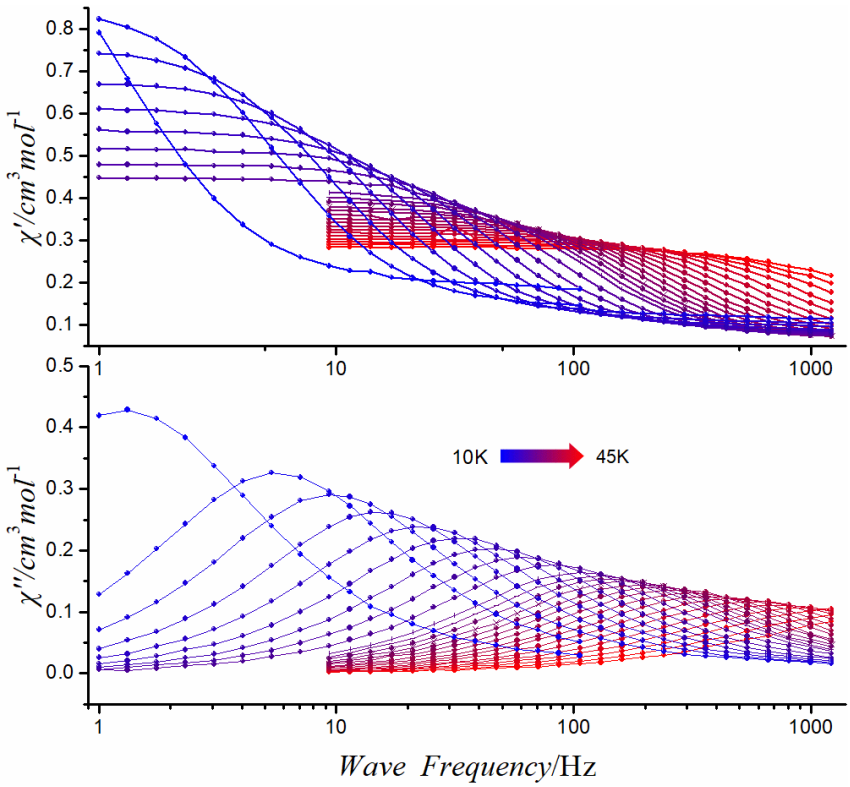

Fig. S6. Variable frequency in-phase (top) and out-of-phase (bottom) magnetic susceptibility of **1**, in zero static field and an oscillating field of 3.5 Oe. Solid lines are fits to the generalized Debye model.

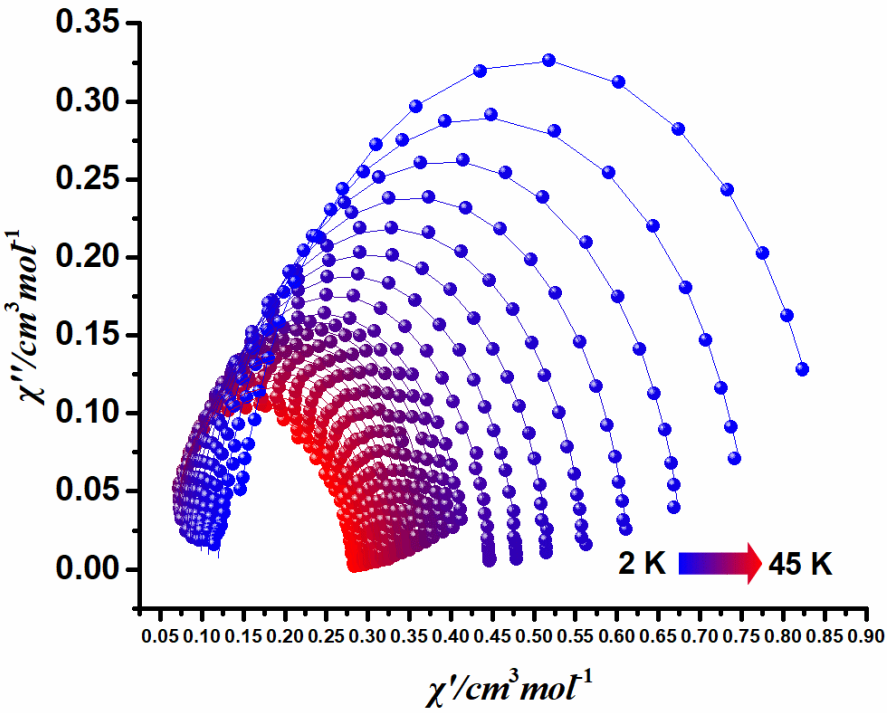

Fig. S7. The Cole-Cole plot of **1** under zero dc field, the solid part is the fitting result.

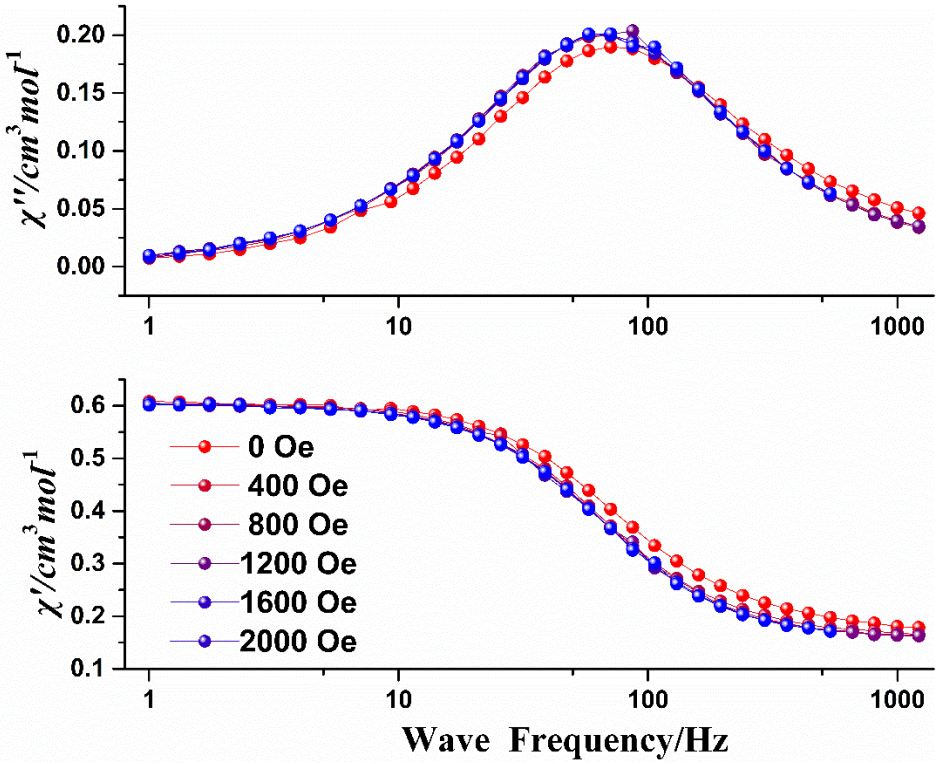

Fig. S8. Frequency dependence of the in-phase (χ') and out-of-phase (χ") ac susceptibility for **1** under different dc fields. The lines are guides to the eyes.

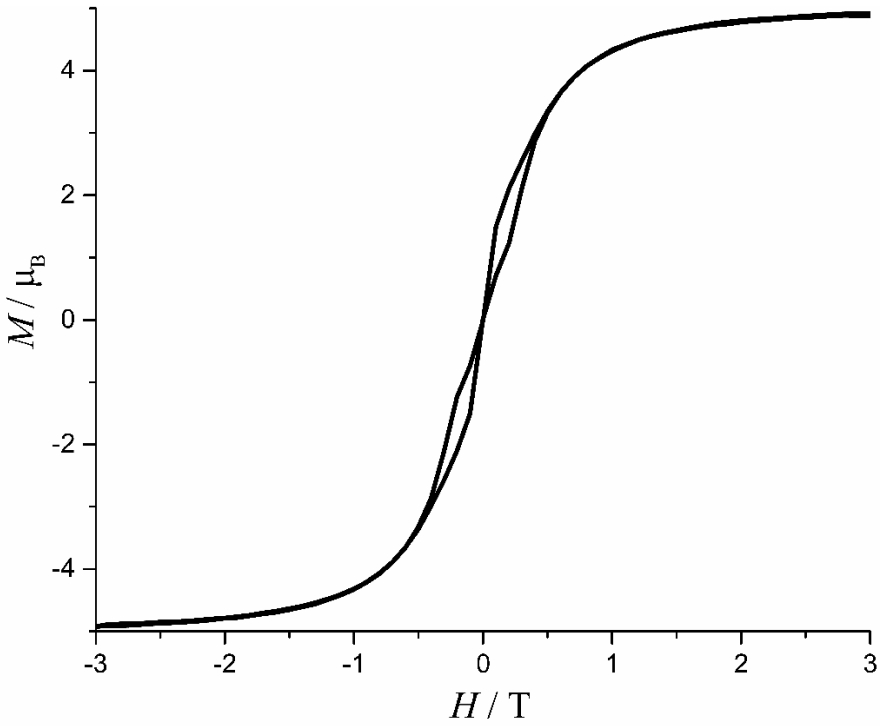

Fig. S9. Magnetic hysteresis of **1** under 2 K.

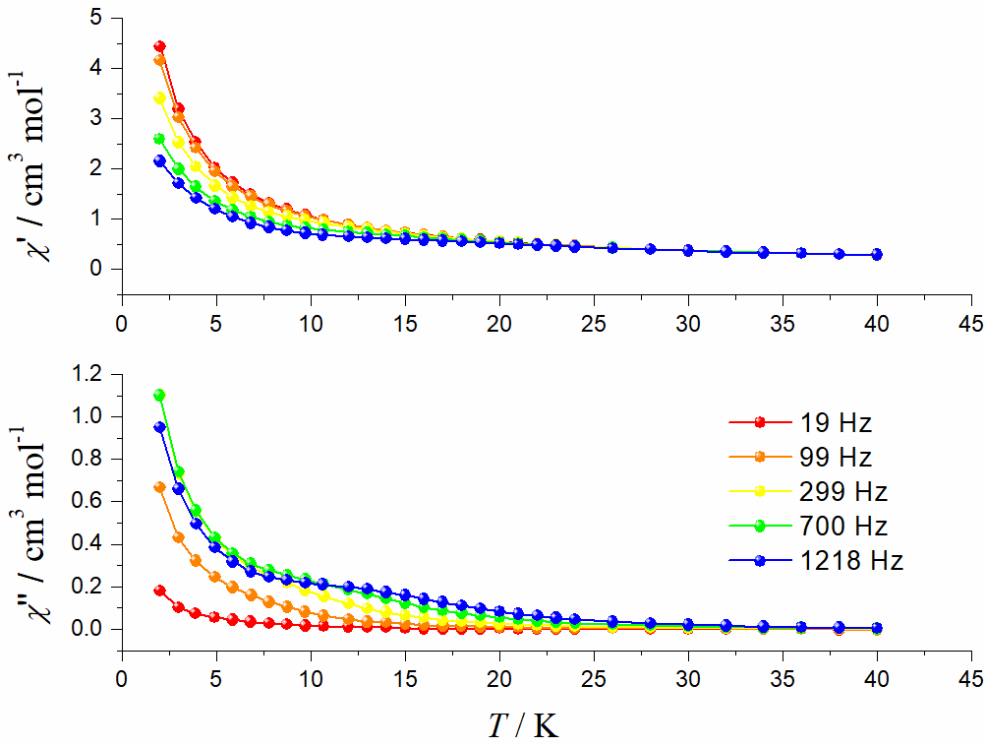

Fig. S10. Variable-temperature in-phase (top) and out-of-phase (bottom) magnetic susceptibility of **2**, in zero static field and an oscillating field of 3.5 Oe.

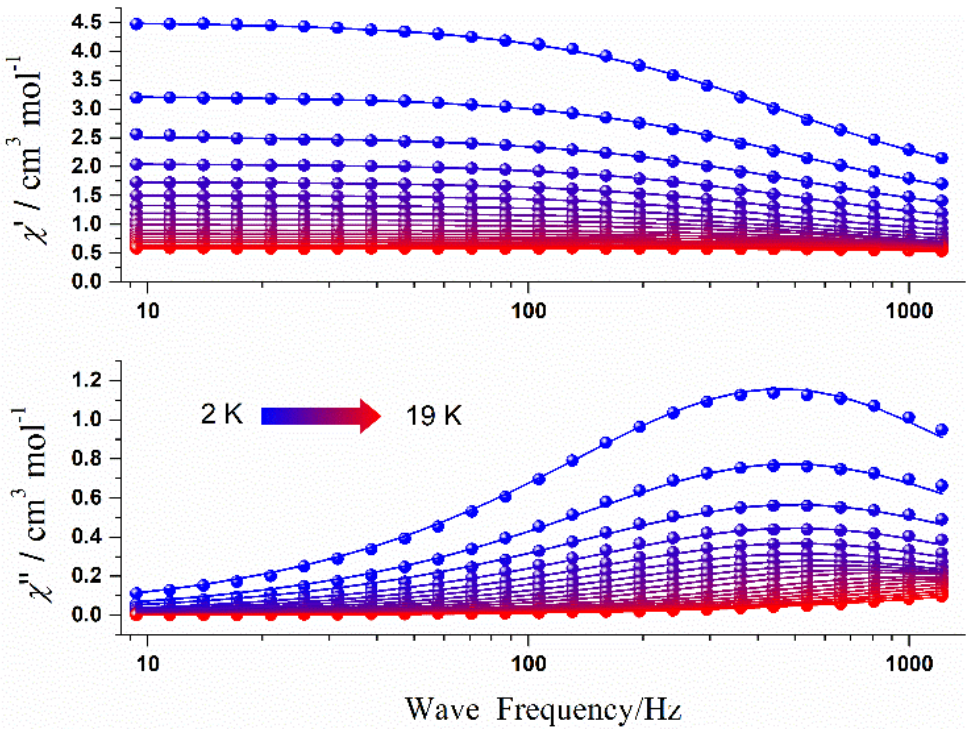

Fig. S11: Variable frequency in-phase (top) and out-of-phase (bottom) magnetic susceptibility of **2**, in zero static field and an oscillating field of 3.5 Oe. Solid lines are fits to the generalized Debye model.

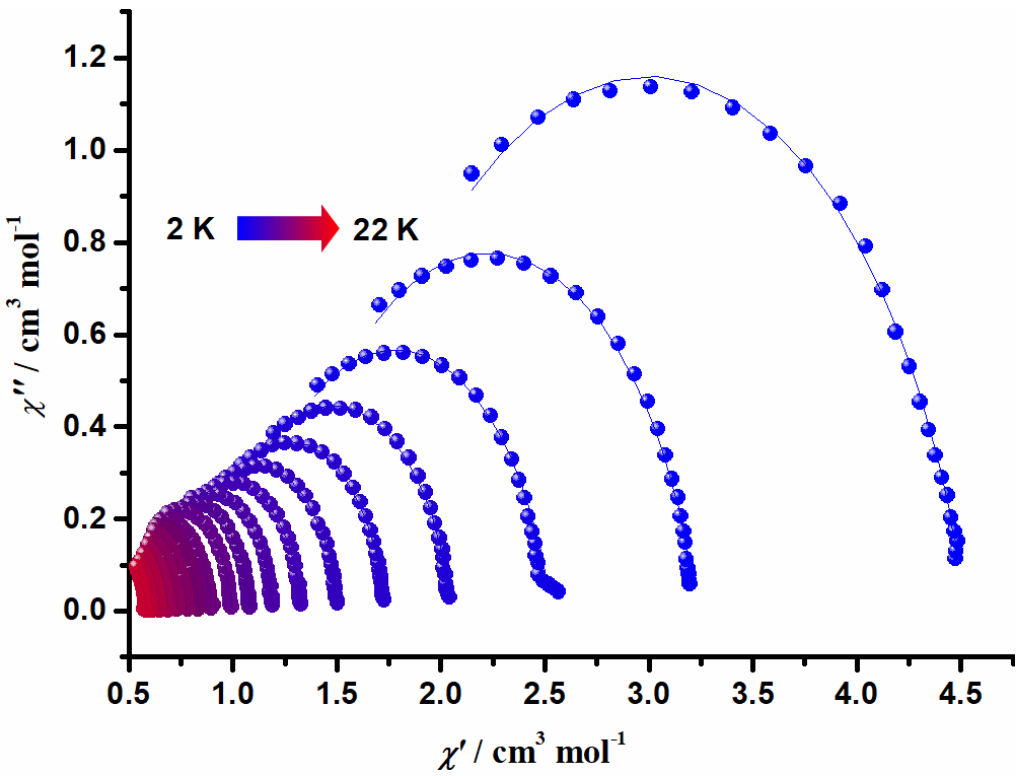

Fig. S12. The Cole-Cole plot of **2** under a dc field of 0 Oe, the solid part is the fitting result.

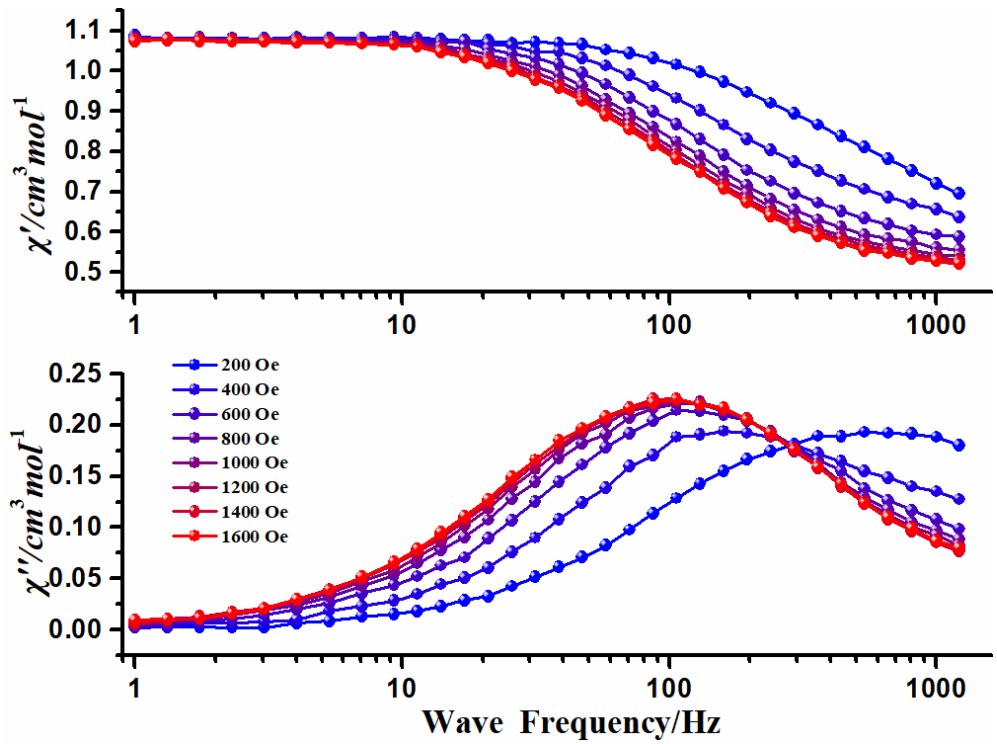

Fig. S13. Frequency dependence of the in-phase (χ') and out-of-phase (χ") ac susceptibility for **2** under different dc fields. The lines are guides to the eyes.

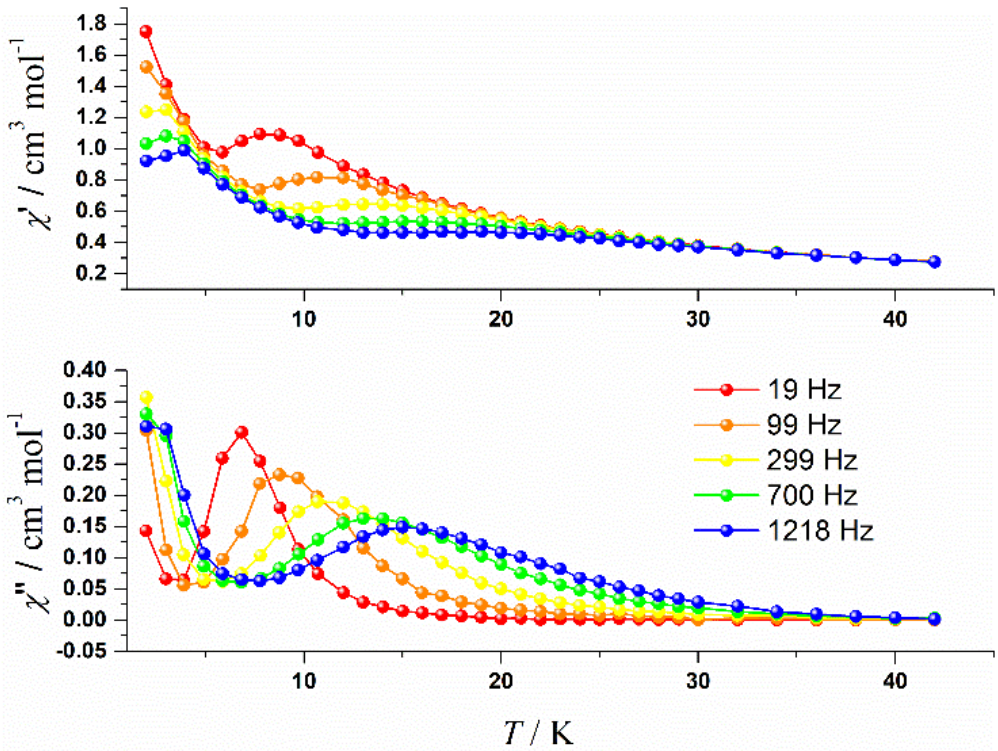

Fig. S14. Variable-temperature in-phase (top) and out-of-phase (bottom) magnetic susceptibility of **2** under a dc field of 1400 Oe.

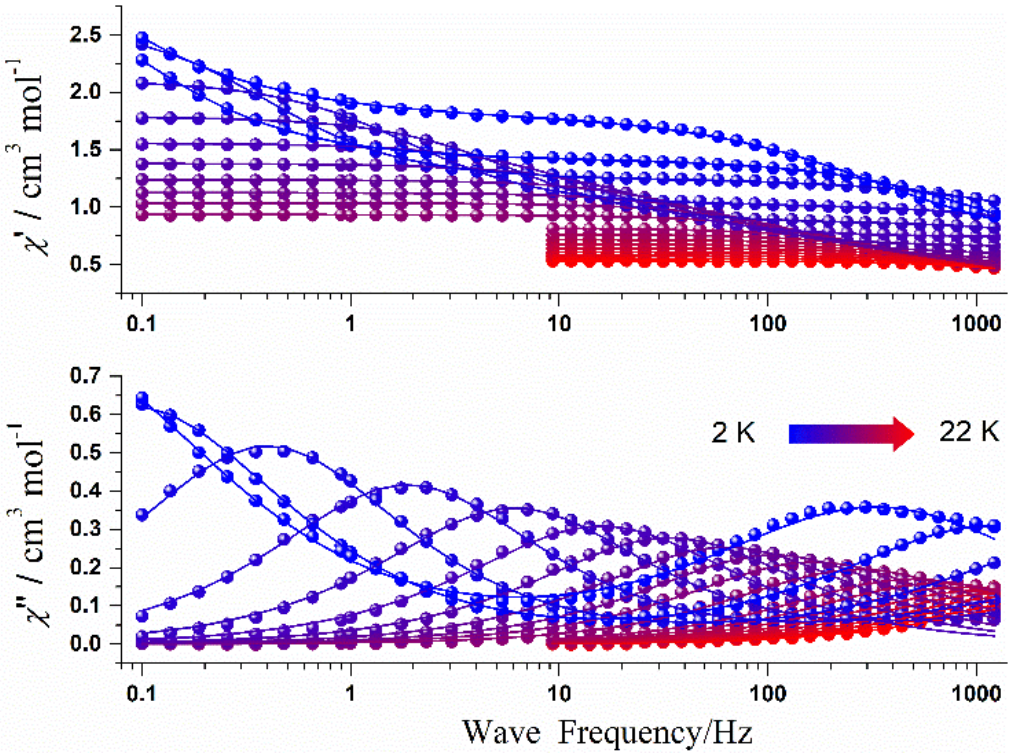

Fig. S15. Variable frequency in-phase (top) and out-of-phase (bottom) magnetic susceptibility of **2** under the dc field of 1400 Oe and an oscillating field of 3.5 Oe. Solid lines are fits to the generalized Debye model.

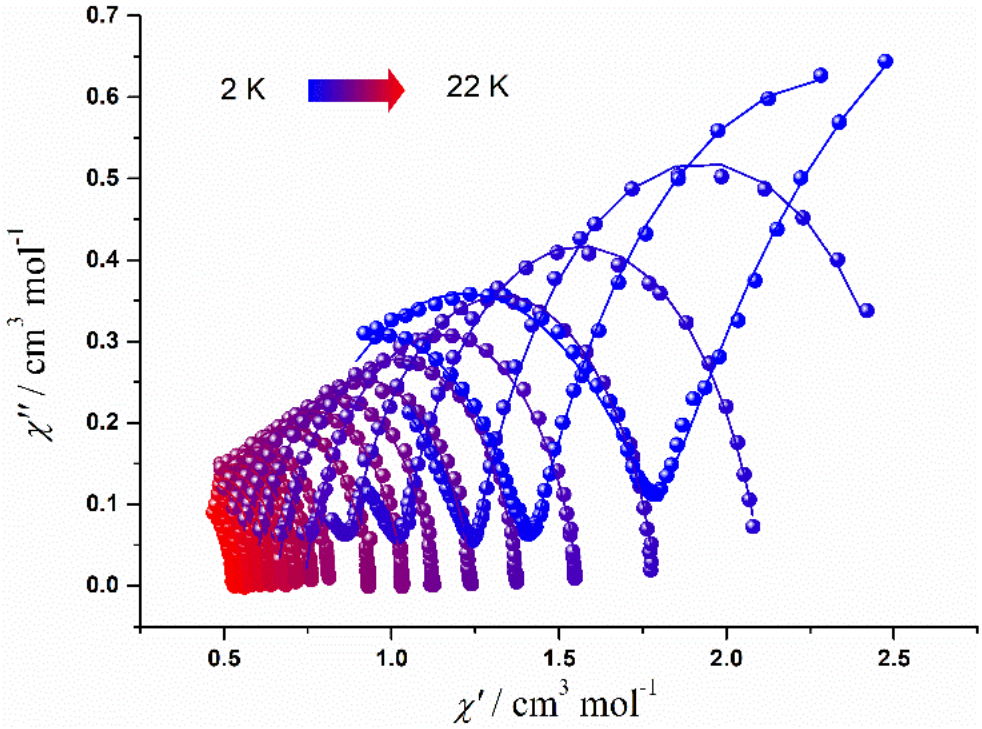

Fig. S16. The Cole-Cole plot of **2** under a dc field of 1400 Oe, the solid part is the fitting result.

Table S6. The fitting parameters of Cole-Cole plot for **1** under zero dc field.

T / K	τ / s	α	χ_S	χ_T
45	5.7182E-5	0.16732	0.01736	0.28523
44	9.50578E-5	0.12769	0.04975	0.29097
43	1.22854E-4	0.12229	0.04445	0.29763
42	1.72419E-4	0.09795	0.05565	0.30384
41	2.21221E-4	0.09792	0.05367	0.31306
40	2.75878E-4	0.08538	0.05171	0.31907
39	3.42352E-4	0.07885	0.05162	0.32681
38	4.24865E-4	0.06643	0.05525	0.33487
37	5.12421E-4	0.05835	0.05665	0.34253
36	6.04304E-4	0.05442	0.05665	0.35227
35	7.13911E-4	0.04828	0.05874	0.36112
34	8.29924E-4	0.04751	0.06014	0.37203
33	9.56034E-4	0.04483	0.06155	0.38086
32	0.00111	0.04386	0.06387	0.39399
31	0.00127	0.04257	0.06543	0.40543
30	0.00146	0.04167	0.06825	0.41861
28	0.00193	0.04444	0.07153	0.44755
26	0.00259	0.04285	0.07762	0.48002
24	0.00353	0.04654	0.08275	0.51762
22	0.00489	0.04959	0.08939	0.56189

20	0.00702	0.05114	0.09786	0.61458
18	0.01038	0.05773	0.10688	0.68015
16	0.01644	0.06719	0.1189	0.76211
14	0.02795	0.06646	0.13855	0.86307

Table S7. The fitting parameters of Cole-Cole plot for **2** under zero dc field.

T / K	τ / s	α	χ_S	χ_T
6	3.115E-4	0.14897	0.80428	1.73733
7	2.98883E-4	0.14106	0.71977	1.51038
8	2.78496E-4	0.1212	0.65339	1.33258
9	2.48096E-4	0.10681	0.59144	1.19502
10	2.17611E-4	0.09381	0.54264	1.08338
11	1.8426E-4	0.08554	0.49418	0.9936
12	1.4753E-4	0.08272	0.44384	0.8962
13	1.25237E-4	0.0733	0.41163	0.83217
14	1.00872E-4	0.08355	0.37042	0.77957
15	8.35495E-5	0.08607	0.34025	0.73078
16	6.82717E-5	0.08989	0.30732	0.68708
17	5.54086E-5	0.09516	0.27963	0.64808
18	4.24036E-5	0.11087	0.23149	0.61449
19	3.80766E-5	0.10625	0.22969	0.58357

Table S8. The fitting parameters of Cole-Cole plot for **2** under 1400 Oe dc field.

T / K	τ / s	α	χ_S	χ_T
22	6.22945E-5	0.10663	0.27432	0.53092
21	7.62794E-5	0.10245	0.29343	0.55425
20	8.41288E-5	0.11158	0.29094	0.58031
19	1.04583E-4	0.11132	0.3108	0.60948
18	1.25248E-4	0.12079	0.32043	0.64292
17	1.51395E-4	0.13142	0.33213	0.67897
16	1.89151E-4	0.13821	0.34864	0.71996
15	2.40134E-4	0.14295	0.36553	0.76569
14	3.1704E-4	0.15021	0.38699	0.81898
12	5.8104E-4	0.14619	0.44222	0.93517
11	9.60911E-4	0.15236	0.48906	1.03636
10	0.00149	0.1514	0.53425	1.1274
9	0.00252	0.15843	0.5881	1.24086
8	0.00472	0.16668	0.65476	1.38094
7	0.01002	0.17824	0.73904	1.55945
6	0.02627	0.19344	0.82137	1.7412
5	0.08529	0.24566	0.92001	1.93563

5. Computation method

5.1 Electronic Structure Calculations.

Ab initio calculations at SA-CASSCF/RASSI level were performed on program MOLCAS 8.0[1] and the structure was originally taken from the X-Ray structure of **1** and **2**. The basis sets were chosen from the ANO-RCC library[2] as have been used in many works[3, 4]. The Dy atom was treated with VTZP quality, then the related Cl and O atoms with VDZP quality and others (C and H atoms) with VDZ quality. The state-averaged CASSCF orbitals of the sextets, quartets and doublets were optimised with 21, 224 and 490 states, respectively, with the RASSCF module. 21, 128 and 130 sextets, quartets and doublets were chosen to constructe and diagonalise in spin-orbit (SO) coupling Hamiltonian with the RASSI4 module. These computed SO states were written into the SINGLE_ANISO[5] program to compute the g-tensors, crystal field parameters, magnetic energy levels for the doublets of the ground J = 15/2 multiplet of the ^{6}H term for Dy(III) and magnetic susceptibility as well as magnetization plot. The two electron integrals were Cholesky decomposed with a threshold of 1×10^{-8} to account for the accuracy.

5.2 DFT Calculations.

DFT calculations were performed using computational package Gaussian 09[6] with density functional methods. The structures were taken from the X-ray crystal structure without optimization. The B3LYP[7] functional has been employed for calculations. The basis sets for Dy(III) were the Cundari–Stevens double-ζ polarization;[8] for the rest of the atoms, the 6-31G basis sets were employed. The bonding analysis was performed employing the program Gauss Sum 2.1[9].

5.3 The rate of thermally assisted tunneling transition.

A recently proposed methodology has been applied to determine the structure of the magnetization blocking barrier in the investigated compounds [10, 11]. That is, the rate of thermally assisted tunneling transition (TAT), which is proportional to $e^{-E/kT}\bar{\mu}^2$ where E is the energy of the doublet, k is the Boltzmann constant, $\bar{\mu}$ is average magnetic moment matrix elements connecting opposite components of the KDs and T is the temperature. For **1**, the ratio of TAT rates in the third to fifth KDs at 40 K (the temperature preceding the linear domain for the τ^{-1} vs. T curve in Fig. 2b), we obtain TAT-5/TAT-4/TAT-3 ≈ 1: 44: 4. This ratio imply that the activated relaxation via the fourth KD becomes dominant in the temperature domain where Orbach process is observed at high temperature. Therefore, the slope of this linear dependence (the height of the barrier) corresponds to the energy of the fourth doublet in full agreement with *ab initio* calculations. For **2**, the situation is much different. The temperature of 15 K will lead the linear domain for the plot, so that the ground QTM effect will be much stronger compared with the higher ones.

Meanwhile, this is clearly shown in the dynamic relaxation with the QTM process in low temperature and hence the U_{eff} (53 K) of **2** is much lower than the calculated first excited doublet (585 K).

5.4 The discussion of electronic structure calculations on 1a and 1b.

In all the studied model complexes, m_J = ±15/2 has been stabilized as the ground state, as presented by real complex **1**, showing a strong axial coordination to the central Dy(III) ion due to its strong oblate character in ±15/2 state. Then m_J = ±13/2 and ±11/2 were both localized in the first and second excited states, respectively, and the transition of magnetic microstates from |±15/2> → |±13/2> → |±11/2> are dominant in the relaxation pathway. However, the differences in the wave function composition of higher excited m_J levels arise. For model **1a**, the third to eighth excited doublets are a high mixture of states due to the low symmetry of the structure and the disturbance of THF ligands. This clearly suggests that the Cl- ions at the equatorial positions stabilize the lower m_J levels, as these levels possess electron density along the axial as well as the equatorial directions. As the Cl^- ions are removed in **1a**, this significantly reduces the charges on the equatorial circle leading to a change in the m_J levels.[13] Even though the tunneling value for **1a** ($2.9 \times 10^{-8}\mu_B{}^2$) decreases significantly compared to **1** ($2.0 \times 10^{-6}\mu_B{}^2$), the presence of non-negligible tunneling values leads to relaxation via the third excited pseudo doublets with a considerable increase (256 K) in the energy barrier for **1a** compared to **1**. As soon as equatorial ligands are eliminated, negligible tunnelling values were obtained for up to sixth excited states, depicting the possibility of relaxation via higher excited states.[14] Based on this, we have constructed a highly symmetric complex $[Dy(Im^{Dipp}N)_2]^+$ **1b**, where m_J = |±15/2> is found to be the ground state as expected, followed by a series of highly pure microstates due to the higher symmetry and stronger donor interaction, which pushes the relaxation further to higher excited doublets as shown in Fig. 5.

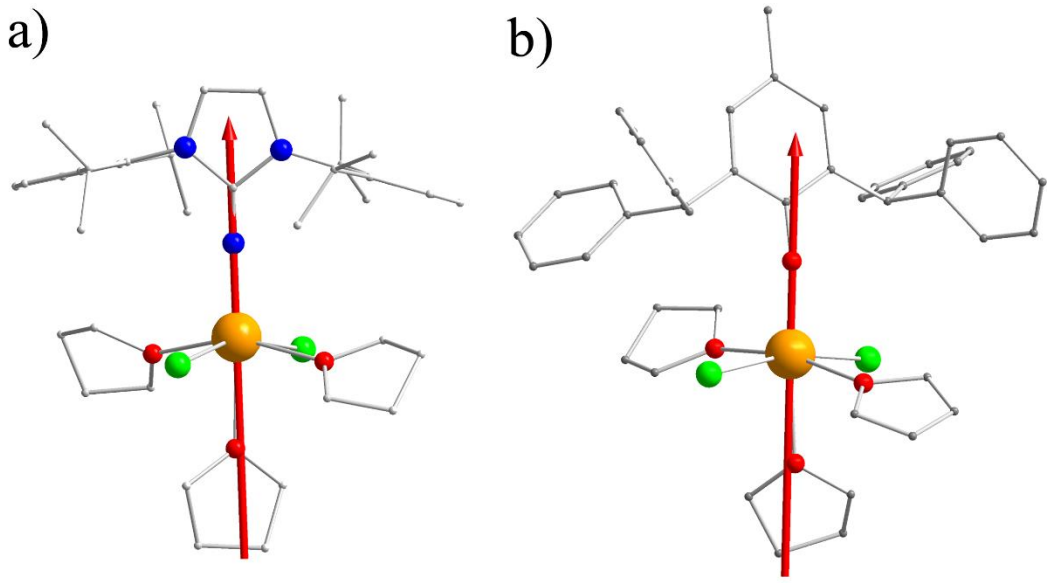

Fig. S17. The principal magnetic axis of the ground Kramers' doublet of **1** (a) and **2** (b).

Table S9. SA-CASSCF/RASSI calculated electronic states for **1**.

Energy (cm $^{-1}$)	Energy (K)	g_x	g_y	g_z	g_z Angle (°)	Wavefunction
0	0	0	0	19.86	--	99.7%|±15/2>
276	397	0.1	0.1	16.88	0.7	97.1%|±13/2>
470	676	2.2	5.8	10.57	9.1	64%|±11/2> + 19%|±3/2>
528	759	8.6	7.2	0.50	89	17%|±11/2> + 12%|±1/2> + 36%|∓1/2> + 14%|∓9/2>
633	910	0.7	2.8	11.98	86	23%|±9/2> + 15%|±5/2> + 33%|∓3/2>
660	949	0.3	1.7	13.73	85	23%|±9/2> + 25%|±5/2> + 28%|∓7/2>
738	1061	1.4	2.0	14.40	88	27%|±9/2> + 10%|±5/2> + 23%|±1/2> + 10%|∓3/2> + 27%|∓7/2>
766	1102	1.3	2.5	16.49	87	34%|±7/2> + 19%|±3/2> + 34%|∓5/2>

[a] Only components with > 10% contribution are given, rounded to the nearest percent.

Table S10. SA-CASSCF/RASSI calculated electronic states for **2**.

Energy (cm $^{-1}$)	Energy (K)	g_x	g_y	g_z	g_z Angle (°)	Wavefunction
0	0	0	0	19.81	--	97.5%|±15/2>
291	418	0.9	1.8	15.85	2.4	86.4%|±13/2>
407	585	2.3	3.8	14.11	88	16%|±11/2> + 25%|±3/2> + 24%|∓1/2>
514	739	9.7	6.2	2.02	83	49%|±11/2> + 24%|∓1/2>
605	870	0.1	2.8	15.80	77	12%|±7/2> + 24%|±5/2> + 15%|±3/2>
646	929	0.5	4.1	13.54	77	13%|±9/2> + 24%|±7/2> + 27%|∓9/2>
695	999	0.4	2.1	15.52	85	12%|±9/2> + 18%|±5/2> + 14%|±3/2> + 13%|∓1/2>
737	1060	0.2	1.7	17.45	68	36%|±7/2> + 21%|±5/2>

[a] Only components with > 10% contribution are given, rounded to the nearest percent.

Table S11. SA-CASSCF/RASSI calculated electronic states for **1a**.

Energy (cm $^{-1}$)	Energy (K)	g_x	g_y	g_z	g_z Angle (°)	Wavefunction
0	0	0	0	19.99	--	99.86%|±15/2>
303	436	0	0	17.30	0.6	99.53%|±13/2>
648	932	0.13	0.16	14.47	1.5	97.54%|±11/2>
858	1234	5.48	6.65	8.99	73	20%|±9/2> + 15%|±1/2> + 24%|∓1/2> + 32%|∓9/2>
929	1336	1.37	4.86	10.19	86	27%|±9/2> + 13%|±1/2> + 36%|∓3/2>
951	1368	0.92	3.29	14.62	86	11%|±9/2> + 24%|±5/2> + 21%|±1/2> + 22%|∓3/2> + 15%|∓7/2>
1035	1488	2.81	4.74	12.09	88	47%|±7/2> + 22%|∓1/2> + 13%|∓5/2>
1075	1546	0.16	1.31	16.15	89	23%|±7/2> + 22%|±3/2> + 44%|∓5/2>

[a] Only components with > 10% contribution are given, rounded to the nearest percent.

Table S12. SA-CASSCF/RASSI calculated electronic states for **1b**.

Energy (cm $^{-1}$)	Energy (K)	g_x	g_y	g_z	g_z Angle (°)	Wavefunction
0	0	0	0	19.91	--	99.99%|±15/2>
819	1178	0	0	16.83	0	99.92%|±13/2>
1570	2258	0	0	13.90	0	99.60%|±11/2>
2174	3126	0	0	11.21	0.4	98.52%|±9/2>
2560	3681	0.26	0.30	8.60	2.9	94.57%|±7/2>
2733	3930	4.67	5.03	6.76	78	53%|±5/2> + 15%|±1/2> + 21%|∓5/2>
2800	4026	1.04	3.91	13.52	89	16%|±5/2> + 19%|±1/2> + 53%|∓3/2>
2856	4107	0.16	0.30	19.29	89	31%|±3/2> + 51%|∓1/2>

[a] Only components with > 10% contribution are given, rounded to the nearest percent.

Table S13. *Ab initio* calculated crystal field parameters for **1**.

Crystal Field Parameter	Value / cm^{-1}
B_2^{-2}	0.38386185576048E-01
B_2^{-1}	0.33040390288394E-02
B_2^{0}	-0.36690756334586E+01
B_2^{1}	-0.25109549389880E-03
B_2^{2}	0.12670193989245E+01
B_4^{-4}	-0.13123216075925E-02
B_4^{-3}	0.17451952510508E-02
B_4^{-2}	-0.46160809827386E-02
B_4^{-1}	0.46377423176558E-02
B_4^{0}	-0.88909802835161E-02
B_4^{1}	0.33911367034557E-03

B_4^2	0.12474069966379E-02
B_4^3	0.20148640830831E-02
B_4^4	-0.37912693515540E-01
B_6^{-6}	-0.34772816824501E-04
B_6^{-5}	0.97129631255562E-04
B_6^{-4}	-0.40270320958349E-04
B_6^{-3}	0.13932789795625E-04
B_6^{-2}	0.13787875625868E-04
B_6^{-1}	-0.42535503123918E-04
B_6^0	0.26707961278586E-04
B_6^1	-0.13843794730029E-04
B_6^2	-0.57024605070370E-04
B_6^3	-0.79852264162827E-05
B_6^4	-0.12508472664088E-03
B_6^5	0.49438891557429E-04
B_6^6	-0.12367496778696E-03

Table S14. *Ab initio* calculated crystal field parameters for **2**.

Crystal Field Parameter	Value / cm^{-1}
B_2^{-2}	0.55212170198238E-01
B_2^{-1}	-0.16107679287045E+00
B_2^0	-0.31886182188864E+01
B_2^1	0.33891420326028E-01
B_2^2	0.15031048487925E+01
B_4^{-4}	0.13429617250154E-02
B_4^{-3}	-0.35712615138237E-02
B_4^{-2}	-0.47794796347089E-02
B_4^{-1}	-0.13688522390070E-01
B_4^0	-0.97542174377553E-02
B_4^1	-0.16569700039991E-01
B_4^2	-0.12336409775194E-02
B_4^3	0.19336820489821E-01
B_4^4	-0.42948684764433E-01
B_6^{-6}	-0.48075089205799E-04
B_6^{-5}	-0.18976616138314E-03
B_6^{-4}	0.13304178016800E-04
B_6^{-3}	-0.27562825523241E-05
B_6^{-2}	0.37138720272824E-04
B_6^{-1}	0.14607746722572E-04
B_6^0	0.18624322140819E-04
B_6^1	0.77406563255457E-04

B_6^2	0.25422372454458E-04
B_6^3	0.14148780071098E-03
B_6^4	-0.17171075995144E-03
B_6^5	-0.33262875761121E-03
B_6^6	0.12163758020887E-03

Table S15. *Ab initio* calculated crystal field parameters for **1a**.

Crystal Field Parameter	Value / cm^{-1}
B_2^{-2}	0.72337001681031E-02
B_2^{-1}	0.15955608115894E-02
B_2^0	-0.59585180633645E+01
B_2^1	-0.70730605445033E-03
B_2^2	0.78827729458104E+00
B_4^{-4}	-0.48163158547002E-03
B_4^{-3}	0.10284888911392E-02
B_4^{-2}	-0.17965861409573E-02
B_4^{-1}	0.15651476101648E-02
B_4^0	-0.91988881401540E-02
B_4^1	0.29064660751428E-02
B_4^2	0.69883964576539E-02
B_4^3	0.15844471487769E-02
B_4^4	-0.29064660751428E-01
B_6^{-6}	-0.14258881411918E-04
B_6^{-5}	0.62899911329782E-05
B_6^{-4}	-0.13654096372133E-04
B_6^{-3}	0.24334102106323E-04
B_6^{-2}	0.15439298332442E-04
B_6^{-1}	-0.12434118863656E-04
B_6^0	0.58116827594653E-04
B_6^1	-0.57375383729070E-04
B_6^2	-0.19121002046725E-04
B_6^3	-0.41509245341708E-05
B_6^4	-0.63206685686162E-05
B_6^5	0.36549435837388E-05
B_6^6	-0.13039037328297E-03

Table S16. *Ab initio* calculated crystal field parameters for **1b**.

Crystal Field Parameter	Value / cm^{-1}
B_2^{-2}	0.23887328816878E-03
B_2^{-1}	-0.18011054286989E-01
B_2^{0}	-0.17216671838758E+02
B_2^{1}	-0.10958051029661E-01
B_2^{2}	0.18221851290563E+01
B_4^{-4}	0.74549504992604E-05
B_4^{-3}	0.34818191459011E-03
B_4^{-2}	0.61251693312660E-04
B_4^{-1}	0.78982178339340E-03
B_4^{0}	-0.11649970626131E-01
B_4^{1}	-0.67349651532058E-04
B_4^{2}	0.48886656704019E-02
B_4^{3}	-0.22938711566715E-03
B_4^{4}	0.48580833715080E-04
B_6^{-6}	-0.48919799944076E-07
B_6^{-5}	-0.49103367351131E-06
B_6^{-4}	0.25018599173407E-07
B_6^{-3}	-0.37716573073922E-05
B_6^{-2}	-0.11613802328768E-05
B_6^{-1}	-0.22029740715458E-04
B_6^{0}	0.70918822935693E-04
B_6^{1}	0.52702776697945E-05
B_6^{2}	-0.13648717628672E-03
B_6^{3}	0.18895059546505E-05
B_6^{4}	-0.36744690724668E-06
B_6^{5}	0.55419388246537E-06
B_6^{6}	-0.47203283164912E-07

Table S17. Average transition magnetic moment elements between the states of **1**, given in μ_B^2.

	$\lvert+\frac{15}{2}\rangle$	$\lvert-\frac{15}{2}\rangle$	$\lvert+\frac{13}{2}\rangle$	$\lvert-\frac{13}{2}\rangle$	$\lvert+\frac{11}{2}\rangle$	$\lvert-\frac{11}{2}\rangle$	$\lvert+a\rangle$	$\lvert-a\rangle$	$\lvert+b\rangle$	$\lvert-b\rangle$	$\lvert+c\rangle$	$\lvert-c\rangle$	$\lvert+d\rangle$	$\lvert-d\rangle$	$\lvert+e\rangle$	$\lvert-e\rangle$
$\lvert+\frac{15}{2}\rangle$	--	2.0E-06	1.6E-04	4.5E+00	4.7E-03	2.1E-03	2.7E-03	1.5E-02	2.8E-03	1.0E-02	1.3E-02	8.3E-03	3.4E-03	8.2E-03	1.7E-03	6.0E-03
$\lvert-\frac{15}{2}\rangle$	2.0E-06	--	4.5E+00	1.6E-04	2.1E-03	4.7E-03	1.5E-02	2.7E-03	1.0E-02	2.8E-03	8.3E-03	1.3E-02	8.2E-03	3.4E-03	6.0E-03	1.7E-03
$\lvert+\frac{13}{2}\rangle$	1.6E-04	4.5E+00	--	5.6E-03	1.6E+00	5.4E+00	5.3E-02	1.2E+00	7.6E-02	2.3E-01	1.3E-01	7.0E-02	7.4E-03	8.6E-02	5.1E-02	2.6E-02
$\lvert-\frac{13}{2}\rangle$	4.5E+00	1.6E-04	5.6E-03	--	5.4E+00	1.6E+00	1.2E+00	5.3E-02	2.3E-01	7.6E-02	7.0E-02	1.3E-01	8.6E-02	7.4E-03	2.6E-02	5.1E-02
$\lvert+\frac{11}{2}\rangle$	4.7E-03	2.1E-03	1.6E+00	5.4E+00	--	9.8E-01	3.7E+00	1.0E+01	4.4E-01	1.1E+00	7.7E-01	5.6E-01	1.3E-01	5.7E-01	2.5E-01	7.1E-02
$\lvert-\frac{11}{2}\rangle$	2.1E-03	4.7E-03	5.4E+00	1.6E+00	9.8E-01	--	1.0E+01	3.7E+00	1.1E+00	4.4E-01	5.6E-01	7.7E-01	5.7E-01	1.3E-01	7.1E-02	2.5E-01
$\lvert+a\rangle$	2.7E-03	1.5E-02	5.3E-02	1.2E+00	3.7E+00	1.0E+01	--	9.2E+00	2.7E+00	4.9E+00	2.6E+00	2.0E+00	4.6E-02	1.7E-02	3.0E-02	2.0E-02
$\lvert-a\rangle$	1.5E-02	2.7E-03	1.2E+00	5.3E-02	1.0E+01	3.7E+00	9.2E+00	--	4.9E+00	2.7E+00	2.0E+00	2.6E+00	1.7E-02	4.6E-02	2.0E-02	3.0E-02
$\lvert+b\rangle$	2.8E-03	1.0E-02	7.6E-02	2.3E-01	4.4E-01	1.1E+00	2.7E+00	4.9E+00	--	9.4E+00	7.7E+00	5.2E-01	1.9E+00	3.2E+00	2.8E-01	1.6E+00
$\lvert-b\rangle$	1.0E-02	2.8E-03	2.3E-01	7.6E-02	1.1E+00	4.4E-01	4.9E+00	2.7E+00	9.4E+00	--	5.2E-01	7.7E+00	3.2E+00	1.9E+00	1.6E+00	2.8E-01
$\lvert+c\rangle$	1.3E-02	8.3E-03	1.3E-01	7.0E-02	7.7E-01	5.6E-01	2.6E+00	2.0E+00	7.7E+00	5.2E-01	--	1.6E+01	1.8E+00	3.0E+00	1.3E+00	1.2E+00
$\lvert-c\rangle$	8.3E-03	1.3E-02	7.0E-02	1.3E-01	5.6E-01	7.7E-01	2.0E+00	2.6E+00	5.2E-01	7.7E+00	1.6E+01	--	3.0E+00	1.8E+00	1.2E+00	1.3E+00
$\lvert+d\rangle$	3.4E-03	8.2E-03	7.4E-03	8.6E-02	1.3E-01	5.7E-01	4.6E-02	1.7E-02	1.9E+00	3.2E+00	1.8E+00	3.0E+00	--	1.8E+01	7.7E+00	1.5E+00
$\lvert-d\rangle$	8.2E-03	3.4E-03	8.6E-02	7.4E-03	5.7E-01	1.3E-01	1.7E-02	4.6E-02	3.2E+00	1.9E+00	3.0E+00	1.8E+00	1.8E+01	--	1.5E+00	7.7E+00
$\lvert+e\rangle$	1.7E-03	6.0E-03	5.1E-02	2.6E-02	2.5E-01	7.1E-02	3.0E-02	2.0E-02	2.8E-01	1.6E+00	1.3E+00	1.2E+00	7.7E+00	1.5E+00	--	2.4E+01
$\lvert-e\rangle$	6.0E-03	1.7E-03	2.6E-02	5.1E-02	7.1E-02	2.5E-01	2.0E-02	3.0E-02	1.6E+00	2.8E-01	1.2E+00	1.3E+00	1.5E+00	7.7E+00	2.4E+01	--

Table S18. Average transition magnetic moment elements between the states of **2**, given in μ_B^2.

	$\lvert+\frac{15}{2}\rangle$	$\lvert-\frac{15}{2}\rangle$	$\lvert+\frac{13}{2}\rangle$	$\lvert-\frac{13}{2}\rangle$	|+a>	|-a>	|+b>	|-b>	|+c>	|-c>	|+d>	|-d>	|+e>	|-e>	|+f>	|-f>
$\lvert+\frac{15}{2}\rangle$	--	1.1E-04	4.4E+00	1.1E-02	9.8E-02	6.8E-02	1.5E-02	1.5E-02	3.7E-03	8.9E-03	2.3E-02	2.0E-02	9.2E-03	4.5E-03	3.6E-03	1.7E-02
$\lvert-\frac{15}{2}\rangle$	1.1E-04	--	1.1E-02	4.4E+00	6.8E-02	9.8E-02	1.5E-02	1.5E-02	8.9E-03	3.7E-03	2.0E-02	2.3E-02	4.5E-03	9.2E-03	1.7E-02	3.6E-03
$\lvert+\frac{13}{2}\rangle$	4.4E+00	1.1E-02	--	5.0E-01	2.2E+00	4.9E+00	2.8E+00	5.4E-01	1.3E-01	2.4E-01	1.4E-02	3.3E-01	7.9E-02	1.3E-01	7.2E-03	1.4E-01
$\lvert-\frac{13}{2}\rangle$	1.1E-02	4.4E+00	5.0E-01	--	4.9E+00	2.2E+00	5.4E-01	2.8E+00	2.4E-01	1.3E-01	3.3E-01	1.4E-02	1.3E-01	7.9E-02	1.4E-01	7.2E-03
|+a>	9.8E-02	6.8E-02	2.2E+00	4.9E+00	--	1.0E+01	5.0E+00	4.2E+00	8.6E-01	1.5E-01	5.7E-01	2.5E-01	1.4E-01	3.0E-01	1.4E-01	1.2E-01
|-a>	6.8E-02	9.8E-02	4.9E+00	2.2E+00	1.0E+01	--	4.2E+00	5.0E+00	1.5E-01	8.6E-01	2.5E-01	5.7E-01	3.0E-01	1.4E-01	1.2E-01	1.4E-01
|+b>	1.5E-02	1.5E-02	2.8E+00	5.4E-01	5.0E+00	4.2E+00	--	9.3E+00	1.5E+00	4.0E+00	4.0E+00	2.3E+00	1.0E+00	4.2E-01	1.2E-01	3.6E-01
|-b>	1.5E-02	1.5E-02	5.4E-01	2.8E+00	4.2E+00	5.0E+00	9.3E+00	--	4.0E+00	1.5E+00	2.3E+00	4.0E+00	4.2E-01	1.0E+00	3.6E-01	1.2E-01
|+c>	3.7E-03	8.9E-03	1.3E-01	2.4E-01	8.6E-01	1.5E-01	1.5E+00	4.0E+00	--	1.7E+00	1.9E+00	3.4E+00	1.9E+00	5.5E-01	2.6E-01	1.0E+00
|-c>	8.9E-03	3.7E-03	2.4E-01	1.3E-01	1.5E-01	8.6E-01	4.0E+00	1.5E+00	1.7E+00	--	3.4E+00	1.9E+00	5.5E-01	1.9E+00	1.0E+00	2.6E-01
|+d>	2.3E-02	2.0E-02	1.4E-02	3.3E-01	5.7E-01	2.5E-01	4.0E+00	2.3E+00	1.9E+00	3.4E+00	--	1.4E+01	4.6E+00	8.1E-01	1.3E+00	1.4E+00
|-d>	2.0E-02	2.3E-02	3.3E-01	1.4E-02	2.5E-01	5.7E-01	2.3E+00	4.0E+00	3.4E+00	1.9E+00	1.4E+01	--	8.1E-01	4.6E+00	1.4E+00	1.3E+00
|+e>	9.2E-03	4.5E-03	7.9E-02	1.3E-01	1.4E-01	3.0E-01	1.0E+00	4.2E-01	1.9E+00	5.5E-01	4.6E+00	8.1E-01	--	1.3E+01	1.5E+00	5.4E+00
|-e>	4.5E-03	9.2E-03	1.3E-01	7.9E-02	3.0E-01	1.4E-01	4.2E-01	1.0E+00	5.5E-01	1.9E+00	8.1E-01	4.6E+00	1.3E+01	--	5.4E+00	1.5E+00
|+f>	3.6E-03	1.7E-02	7.2E-03	1.4E-01	1.4E-01	1.2E-01	1.2E-01	3.6E-01	2.6E-01	1.0E+00	1.3E+00	1.4E+00	1.5E+00	5.4E+00	--	1.0E+01
|-f>	1.7E-02	3.6E-03	1.4E-01	7.2E-03	1.2E-01	1.4E-01	3.6E-01	1.2E-01	1.0E+00	2.6E-01	1.4E+00	1.3E+00	5.4E+00	1.5E+00	1.0E+01	--

Table S19. Average transition magnetic moment elements between the states of **1a**, given in μ_B^2.

	$\lvert+\frac{15}{2}\rangle$	$\lvert-\frac{15}{2}\rangle$	$\lvert+\frac{13}{2}\rangle$	$\lvert-\frac{13}{2}\rangle$	$\lvert+\frac{11}{2}\rangle$	$\lvert-\frac{11}{2}\rangle$	$\lvert+a\rangle$	$\lvert-a\rangle$	$\lvert+b\rangle$	$\lvert-b\rangle$	$\lvert+c\rangle$	$\lvert-c\rangle$	$\lvert+d\rangle$	$\lvert-d\rangle$	$\lvert+e\rangle$	$\lvert-e\rangle$
$\lvert+\frac{15}{2}\rangle$	--	2.9E-08	2.9E-04	4.5E+00	5.2E-03	1.9E-06	9.0E-04	5.3E-04	8.6E-04	1.0E-04	3.2E-04	6.8E-04	5.5E-04	3.1E-04	3.2E-04	6.1E-04
$\lvert-\frac{15}{2}\rangle$	2.9E-08	--	4.5E+00	2.9E-04	1.9E-06	5.2E-03	5.3E-04	9.0E-04	1.0E-04	8.6E-04	6.8E-04	3.2E-04	3.1E-04	5.5E-04	6.1E-04	3.2E-04
$\lvert+\frac{13}{2}\rangle$	2.9E-04	4.5E+00	--	6.4E-03	5.7E-04	8.3E+00	1.7E-03	3.0E-03	1.9E-02	3.3E-03	1.3E-02	1.2E-02	2.6E-04	1.3E-02	6.1E-03	4.4E-03
$\lvert-\frac{13}{2}\rangle$	4.5E+00	2.9E-04	6.4E-03	--	8.3E+00	5.7E-04	3.0E-03	1.7E-03	3.3E-03	1.9E-02	1.2E-02	1.3E-02	1.3E-02	2.6E-04	4.4E-03	6.1E-03
$\lvert+\frac{11}{2}\rangle$	5.2E-03	1.9E-06	5.7E-04	8.3E+00	--	3.8E-03	4.9E+00	3.1E+00	2.3E+00	1.3E-01	1.1E+00	5.7E-02	4.0E-02	2.9E-01	5.8E-02	1.2E-02
$\lvert-\frac{11}{2}\rangle$	1.9E-06	5.2E-03	8.3E+00	5.7E-04	3.8E-03	--	3.1E+00	4.9E+00	1.3E-01	2.3E+00	5.7E-02	1.1E+00	2.9E-01	4.0E-02	1.2E-02	5.8E-02
$\lvert+a\rangle$	9.0E-04	5.3E-04	1.7E-03	3.0E-03	4.9E+00	3.1E+00	--	6.8E+00	4.2E+00	5.6E+00	1.9E+00	3.2E+00	7.8E-01	3.7E-01	2.5E-01	4.1E-01
$\lvert-a\rangle$	5.3E-04	9.0E-04	3.0E-03	1.7E-03	3.1E+00	4.9E+00	6.8E+00	--	5.6E+00	4.2E+00	3.2E+00	1.9E+00	3.7E-01	7.8E-01	4.1E-01	2.5E-01
$\lvert+b\rangle$	8.6E-04	1.0E-04	1.9E-02	3.3E-03	2.3E+00	1.3E-01	4.2E+00	5.6E+00	--	9.7E+00	1.1E+00	4.7E+00	6.3E+00	2.1E+00	2.8E-01	2.1E-01
$\lvert-b\rangle$	1.0E-04	8.6E-04	3.3E-03	1.9E-02	1.3E-01	2.3E+00	5.6E+00	4.2E+00	9.7E+00	--	4.7E+00	1.1E+00	2.1E+00	6.3E+00	2.1E-01	2.8E-01
$\lvert+c\rangle$	3.2E-04	6.8E-04	1.3E-02	1.2E-02	1.1E+00	5.7E-02	1.9E+00	3.2E+00	1.1E+00	4.7E+00	--	1.8E+01	2.0E+00	7.4E-01	1.7E+00	2.5E+00
$\lvert-c\rangle$	6.8E-04	3.2E-04	1.2E-02	1.3E-02	5.7E-02	1.1E+00	3.2E+00	1.9E+00	4.7E+00	1.1E+00	1.8E+01	--	7.4E-01	2.0E+00	2.5E+00	1.7E+00
$\lvert+d\rangle$	5.5E-04	3.1E-04	2.6E-04	1.3E-02	4.0E-02	2.9E-01	7.8E-01	3.7E-01	6.3E+00	2.1E+00	2.0E+00	7.4E-01	--	1.4E+01	8.5E+00	2.0E+00
$\lvert-d\rangle$	3.1E-04	5.5E-04	1.3E-02	2.6E-04	2.9E-01	4.0E-02	3.7E-01	7.8E-01	2.1E+00	6.3E+00	7.4E-01	2.0E+00	1.4E+01	--	2.0E+00	8.5E+00
$\lvert+e\rangle$	3.2E-04	6.1E-04	6.1E-03	4.4E-03	5.8E-02	1.2E-02	2.5E-01	4.1E-01	2.8E-01	2.1E-01	1.7E+00	2.5E+00	8.5E+00	2.0E+00	--	1.9E+01
$\lvert-e\rangle$	6.1E-04	3.2E-04	4.4E-03	6.1E-03	1.2E-02	5.8E-02	4.1E-01	2.5E-01	2.1E-01	2.8E-01	2.5E+00	1.7E+00	2.0E+00	8.5E+00	1.9E+01	--

Table S20. Average transition magnetic moment elements between the states of **1b**, given in μ_B^2.

	$\lvert+\frac{15}{2}\rangle$	$\lvert-\frac{15}{2}\rangle$	$\lvert+\frac{13}{2}\rangle$	$\lvert-\frac{13}{2}\rangle$	$\lvert+\frac{11}{2}\rangle$	$\lvert-\frac{11}{2}\rangle$	$\lvert+\frac{9}{2}\rangle$	$\lvert-\frac{9}{2}\rangle$	$\lvert+\frac{7}{2}\rangle$	$\lvert-\frac{7}{2}\rangle$	$\lvert+a\rangle$	$\lvert-a\rangle$	$\lvert+b\rangle$	$\lvert-b\rangle$	$\lvert+c\rangle$	$\lvert-c\rangle$
$\lvert+\frac{15}{2}\rangle$	--	--	4.4E+00	--	1.4E-04	--	2.1E-03	4.2E-10	1.5E-09	2.9E-07	3.3E-06	8.7E-06	1.4E-07	1.8E-06	8.1E-08	6.9E-07
$\lvert-\frac{15}{2}\rangle$	--	--	--	4.4E+00	--	1.4E-04	4.2E-10	2.1E-03	2.9E-07	1.5E-09	8.7E-06	3.3E-06	1.8E-06	1.4E-07	6.9E-07	8.1E-08
$\lvert+\frac{13}{2}\rangle$	4.4E+00	--	--	--	8.3E+00	--	1.9E-03	4.4E-10	4.2E-08	5.6E-03	7.3E-06	9.7E-06	1.0E-04	1.1E-05	3.2E-05	3.4E-06
$\lvert-\frac{13}{2}\rangle$	--	4.4E+00	--	--	--	8.3E+00	4.4E-10	1.9E-03	5.6E-03	4.2E-08	9.7E-06	7.3E-06	1.1E-05	1.0E-04	3.4E-06	3.2E-05
$\lvert+\frac{11}{2}\rangle$	1.4E-04	--	8.3E+00	--	--	--	1.2E+01	2.3E-06	3.3E-06	9.8E-03	5.1E-03	1.3E-02	2.2E-04	2.6E-03	1.1E-04	9.8E-04
$\lvert-\frac{11}{2}\rangle$	--	1.4E-04	--	8.3E+00	--	--	2.3E-06	1.2E+01	9.8E-03	3.3E-06	1.3E-02	5.1E-03	2.6E-03	2.2E-04	9.8E-04	1.1E-04
$\lvert+\frac{9}{2}\rangle$	2.1E-03	4.2E-10	1.9E-03	4.4E-10	1.2E+01	2.3E-06	--	1.1E-05	1.2E-04	1.4E+01	1.2E-02	3.3E-02	8.3E-02	9.7E-03	2.3E-02	2.6E-03
$\lvert-\frac{9}{2}\rangle$	4.2E-10	2.1E-03	4.4E-10	1.9E-03	2.3E-06	1.2E+01	1.1E-05	--	1.4E+01	1.2E-04	3.3E-02	1.2E-02	9.7E-03	8.3E-02	2.6E-03	2.3E-02
$\lvert+\frac{7}{2}\rangle$	1.5E-09	2.9E-07	4.2E-08	5.6E-03	3.3E-06	9.8E-03	1.2E-04	1.4E+01	--	1.1E-02	1.1E+01	4.3E+00	1.1E+00	1.4E-01	2.4E-01	3.7E-02
$\lvert-\frac{7}{2}\rangle$	2.9E-07	1.5E-09	5.6E-03	4.2E-08	9.8E-03	3.3E-06	1.4E+01	1.2E-04	1.1E-02	--	4.3E+00	1.1E+01	1.4E-01	1.1E+00	3.7E-02	2.4E-01
$\lvert+a\rangle$	3.3E-06	8.7E-06	7.3E-06	9.7E-06	5.1E-03	1.3E-02	1.2E-02	3.3E-02	1.1E+01	4.3E+00	--	4.1E+00	6.9E+00	7.8E+00	2.3E-01	5.2E-01
$\lvert-a\rangle$	8.7E-06	3.3E-06	9.7E-06	7.3E-06	1.3E-02	5.1E-03	3.3E-02	1.2E-02	4.3E+00	1.1E+01	4.1E+00	--	7.8E+00	6.9E+00	5.2E-01	2.3E-01
$\lvert+b\rangle$	1.4E-07	1.8E-06	1.0E-04	1.1E-05	2.2E-04	2.6E-03	8.3E-02	9.7E-03	1.1E+00	1.4E-01	6.9E+00	7.8E+00	--	1.5E+01	1.1E+00	4.1E+00
$\lvert-b\rangle$	1.8E-06	1.4E-07	1.1E-05	1.0E-04	2.6E-03	2.2E-04	9.7E-03	8.3E-02	1.4E-01	1.1E+00	7.8E+00	6.9E+00	1.5E+01	--	4.1E+00	1.1E+00
$\lvert+c\rangle$	8.1E-08	6.9E-07	3.2E-05	3.4E-06	1.1E-04	9.8E-04	2.3E-02	2.6E-03	2.4E-01	3.7E-02	2.3E-01	5.2E-01	1.1E+00	4.1E+00	--	2.9E+01
$\lvert-c\rangle$	6.9E-07	8.1E-08	3.4E-06	3.2E-05	9.8E-04	1.1E-04	2.6E-03	2.3E-02	3.7E-02	2.4E-01	5.2E-01	2.3E-01	4.1E+00	1.1E+00	2.9E+01	--

6. References

1. F. Aquilante, J. Autschbach, R. K. Carlson, L. F. Chibotaru, M. G. Delcey, L. De Vico, I. Fdez. Galván, N. Ferré, L. M. Frutos, L. Gagliardi, M. Garavelli, A. Giussani, C. E. Hoyer, G. Li Manni, H. Lischka, D. Ma, P. Å. Malmqvist, T. Müller, A. Nenov, M. Olivucci, T. B. Pedersen, D. Peng, F. Plasser, B. Pritchard, M. Reiher, I. Rivalta, I. Schapiro, J. Segarra-Martí, M. Stenrup, D. G. Truhlar, L. Ungur, A. Valentini, S. Vancoillie, V. Veryazov, V. P. Vysotskiy, O. Weingart, F. Zapata and R. Lindh, *J. Comput. Chem.*, 2016, **37**, 506–541.
2. B. O. Roos, R. Lindh, P.-Å. Malmqvist, V. Veryazov and P.-O. Widmark, *J. Phys. Chem. A*, 2004, **108**, 2851–2858.
3. C. A. Goodwin, F. Ortu, D. Reta, N. F. Chilton, D. P. Mills, *Nature*, 2017, **548**, 439-442;
4. P. A. Malmqvist, B. O. Roos, B. Schimmelpfennig. *Chem. Phys. Lett.*, 2002, **357**, 230−240.
5. B. O. Roos, R. Lindh, P.-Å. Malmqvist, V. Veryazov and P.-O. Widmark, *Chem. Phys. Lett.*, 2005, **409**, 295–299.
6. Frisch, M. J.; Trucks, G. W.; Schlegel, H. B.; Scuseria, G. E.; Robb, M. A.; Cheeseman, J. R.; Scalmani, G.; Barone, V.; Mennucci, B.; Petersson, G. A.; Nakatsuji, H.; Caricato, M.; Li, X.; Hratchian, H. P.; Izmaylov, A. F.; Bloino, J.; Zheng, G.; Sonnenberg, J. L.; Hada, M.; Ehara, M.; Toyota, K.; Fukuda, R.; Hasegawa, J.; Ishida, M.; Nakajima, T.; Honda, Y.; Kitao, O.; Nakai, H.; Vreven, T.; Montgomery, J. A., Jr.; Peralta, J. E.; Ogliaro, F.; Bearpark, M.; Heyd, J. J.; Brothers, E.; Kudin, K. N.; Staroverov, V. N.; Kobayashi, R.; Normand, J.; Raghavachari, K.; Rendell, A.; Burant, J. C.; Iyengar, S. S.; Tomasi, J.; Cossi, M.; Rega, N.; Millam, N. J.; Klene, M.; Knox, J. E.; Cross, J. B.; Bakken, V.; Adamo, C.; Jaramillo, J.; Gomperts, R.; Stratmann, R. E.; Yazyev, O.; Austin, A. J.; Cammi, R.; Pomelli, C.; Ochterski, J. W.; Martin, R. L.; Morokuma, K.; Zakrzewski, V. G.; Voth, G. A.; Salvador, P.; Dannenberg, J. J.; Dapprich, S.; Daniels, A. D.; Farkas, Ö.; Foresman, J. B.; Ortiz, J. V.; Cioslowski, J.; Fox, D. J. Gaussian 09; Gaussian, Inc.: Wallingford, CT, 2009.
7. a) Stephens, P. J.; Devlin, F. J.; Chabalowski, C. F.; Frisch, M. J. J. *Phys. Chem*. 1994, **98**, 11623−11627; b) Becke, A. D. J. *Chem. Phys*. 1993, **98**, 5648−5652; c) Lee, C. T.; Yang, W. T.; Parr, R. G. *Phys. Rev. B*, 1988, **37**, 785−789; d) Becke, A. D. *Phys. Rev. A*, 1988, **38**, 3098−3100.
8. Cundari, T. R.; Stevens, W. J. J. *Chem. Phys*., 1993, **98**, 5555−5565.
9. a) O'Boyle, N. M. GaussSum 2.1; 2007; available at http://gausssum.sf.net; b) O'Boyle, N. M.; Tenderholt, A. L.; Langner, K. M. *J. Comput. Chem*., 2008, **29**, 839.
10. Ungur, L.; Thewissen, M.; Costes, J.-P.; Wernsdorfer, W.; Chibotaru, L. F. *Inorg. Chem*. 2013, **52**, 6328.
11. Garanin, D. A.; Chudnovsky, E. M. Phys. Rev. B: Condens. *Matter Mater. Phys.* 1997, **56**, 11102.
12. a) N. F. Chilton, C. A. P. Goodwin, D. P. Mills, R. E. P. Winpenny, *Chem. Commun.* 2015, **51**, 101–103; b) N. F. Chilton, *Inorg. Chem.*,2015, **54**, 2097–2099; c) S. K. Singh, T. Gupta, G. Rajaraman, *Inorg. Chem*. 2014, **53**, 10835–10845.
13. S. K. Gupta, T. Rajeshkumar, G. Rajaraman, R. Murugavel, *Chem. Commun.* 2016, **52**, 7168–7171.

14. T. Gupta and G. Rajaraman, *J. Chem. Sci.* 2014, **126**, 1569–1579.